Pergamon

Int. J. Heat Mass Transfer. Vol. 37, No. 8, pp. 1181–1191, 1994

0017-9310/94 $7.00 + 0.00

0017-9310(93)E0085-U

Modelling of combustion and heat transfer in a packed bed with embedded coolant tubes

A. A. MOHAMAD, S. RAMADHYANI and R. VISKANTA
Heat Transfer Laboratory, School of Mechanical Engineering, Purdue University, West Lafayette, IN 47907, U.S.A.

(*Received* 2 *November* 1992 *and in final form* 12 *November* 1993)

Abstract—A model has been developed to simulate combustion and heat transfer in a porous matrix combustor–heater. The system consists of a packed bed in which a premixed natural gas–air mixture combusts. Radiative and convective heat transfer occurs from the flame zone to a fluid flowing through a bank of tubes embedded in the packed bed. Radiative heat transfer in the bed is modelled as a diffusion process, and the flow field and temperature distribution in the bed are calculated. The numerically obtained results are compared with available experimental data for a similar system.

INTRODUCTION

RECENTLY, attention has been focused on the use of porous materials to enhance the efficiency of combustion systems [1–3]. Interest in the development of advanced combustion systems has been motivated by the need for more efficient heat transfer with low emissions of NO_x and other pollutants [4]. The large demand for natural gas for process heating applications provides the impetus for the present study. In conventional process heaters, NO_x is generated by the high temperatures associated with the flame zone, while the presence of cold heat exchanger surfaces within the combustion zone results in flame quenching and increased carbon monoxide and total hydrocarbon emissions.

In the combustor–heater system described in this paper, the premixed reactants are constrained to flow through, and burn within, a porous matrix. Heat is transferred from the hot combustion gases and the porous matrix to a bundle of tubes embedded in the matrix. The tubes carry the process fluid to be heated. Because of the strong emission of radiation from the solid matrix, energy from the high-temperature post-flame zone is fed back to heat the preflame zone of the porous material [5]. This internal heat feedback mechanism results in several advantages relative to a conventional burner [6], including increased burning rates, increased flame stability, the ability to achieve a high heat release rate in a compact combustor, and reduced NO_x formation due to decreased combustion zone temperature. In addition, the porous matrix promotes dispersion of the unreacted carbon monoxide and hydrocarbons in the boundary layers adjacent to embedded heat exchanger surfaces, thus leading to reduced emissions of carbon monoxide and hydrocarbons. Since porous materials of different properties can be used, the temperature profile in the heater can be controlled in such a way as to minimize total emissions. Thus, the concept of combustion in a porous material can provide the basis for development of more efficient combustion systems with ultra-low pollutant emissions. Applications for the idea include boilers, water heaters, thermal fluid heaters, air heaters for industrial and domestic applications, steam generators for enhanced oil recovery, and steam superheaters for waste-to-energy systems [7].

The purpose of this paper is to develop a mathematical model to investigate the thermal performance of a combustor–heater system consisting of a packed bed with two rows of embedded cooling tubes. Premixed natural gas and air flow through the packed bed and combustion takes place within the bed. Fluid flow, heat transfer and combustion are simulated in the porous matrix. The system is governed by a large number of parameters, including the particle diameter, thermophysical properties of the porous matrix, cooling tube diameter, tube shapes and their arrangements, number of tube rows and operating conditions such as firing rate, excess air ratio, etc. The effects of excess air, particle diameter, firing rate, tube spacing, activation energy, and thermal conductivity are studied in this work. The predictions include the flame location, pressure drop, heat transfer rate to the embedded tubes, and the thermal efficiency of the system. Inasmuch as the present effort represents the first attempt at modelling the system, some of the more intractable aspects of the problem, including the prediction of pollutant emissions, are the subjects of ongoing investigations and will be addressed in a subsequent paper.

PROBLEM FORMULATION

Model equations

The coolant flows through a bank of tubes embedded in the porous medium. Premixed fuel and air enter the system through a water-cooled grate at the bottom, as shown in Fig. 1, and combustion takes

NOMENCLATURE

A	pre-exponential factor (1×10^{10} m^3 kg^{-1} s^{-1})
a, b	Ergun's empirical constants ($a=215$, $b=1.8$)
c_{pf}	specific heat of fluid [J kg^{-1} K^{-1}]
D	tube diameter [mm]
Da	Darcy number, K/D^2
D_{AB}	binary diffusion coefficient [m^2 s^{-1}]
d_p	particle diameter [mm]
E	activation energy [J kmol^{-1}]
f	inertia coefficient, $b\phi^{-3/2}/\sqrt{a}$
Fr	Froude number, $V_{in}/\sqrt{(gD)}$
g	acceleration due to gravity [m s^{-2}]
h_c	heat transfer coefficient [W m^{-2} K^{-1}]
h_f	enthalpy of fluid [J kg^{-1}]
H	height of the packed bed [mm]
H_f	dimensionless enthalpy of the fluid, $h_f/\Delta H_c$
H_1, H_2	dimensions shown in Fig. 2 [mm]
K	permeability of the porous medium, $\phi^3 d_p^2/a(1-\phi)^2$ [m^2]
k_{eff}	effective thermal conductivity [W m^{-1} K^{-1}]
k_f	thermal conductivity of the fluid [W m^{-1} K^{-1}]
k_s	thermal conductivity of the solid [W m^{-1} K^{-1}]
m_f	mass fraction of the fuel
m_{ox}	mass fraction of the oxygen
Pr	Prandtl number
p	pressure [Pa]
P	dimensionless pressure, $p/\rho V_{in}^2$
Q_c	heat released by combustion [kW]
Q_t	total heat absorbed by grate and tubes [kW]
R	universal gas constant, 8314 J kmol^{-1} K^{-1}
$R_{contact}$	thermal contact resistance [m^2 K W^{-1}]
Re	Reynolds number, $\rho V_{in} D/\mu$
R_s	volumetric stoichiometric air/fuel ratio
R_x	volumetric air/fuel ratio
r_i	inside tube diameter [m]
r_o	outside tube diameter [m]
Sc	Schmidt number $\mu/\rho D_{AB}$
S_{fu}	rate of fuel consumption [kg m^{-2} s^{-1}]
S_{fu}^*	dimensionless rate of fuel consumption, $S_{fu}D/\rho V_{in}$
T	temperature [K]
T_{ad}	adiabatic flame temperature, 2230 K
u, v	superficial velocity components [m s^{-1}]
U, V	u/V_{in}, v/V_{in}
V_{in}	inlet velocity
$\lvert\mathbf{v}\rvert$	$\sqrt{(u^2+v^2)}$
x, y	coordinate system [mm]
y_f	flame location.

Greek symbols

α_{eff}	effective absorptivity
ΔH_c	heat of combustion [J kg^{-1}]
ε	emissivity
η_{th}	thermal efficiency, (Q_t/Q_c)
θ	dimensionless temperature, $(T-T_{in})/(T_{ad}-T_{in})$
μ	mixture viscosity [kg m^{-1} s^{-1}]
ξ, η	x/H, y/H
ρ	mixture density [kg m^{-3}]
ρ_a°	air density at the reference temperature, 228 K
ρ_g°	fuel density at the reference temperature (288 K), 0.719 kg m^{-3}
ϕ	porosity
ψ	excess air.

Subscripts

a	air
c	coolant
eff	effective
f	fluid
g	products of combustion of a stoichiometric mixture
in	inlet condition
o	outlet condition
s	solid.

place in the porous material. It is assumed that the flow is steady, two-dimensional, compressible, and Newtonian, while the porous material is homogeneous and isotropic. The thermophysical properties of the fluid and the solid matrix are functions of temperature and composition, in general. The combustion reaction is assumed to occur in a single step according to the chemical equation

$$CH_4+2(1+\psi)(O_2+3.76N_2)\rightarrow CO_2+2H_2O+2\psi O_2+7.52(1+\psi)N_2 \quad (1)$$

where ψ represents the proportion of excess air in the reactant stream at the inlet to the system. For convenience, the numerical values of ψ are presented as percentages in this paper. The rate of the reaction is computed through a one-step expression that will shortly be presented. The geometrical complexity of the system requires detailed two-dimensional calculations of the velocity and temperature fields. To keep the computational effort within manageable proportions, the chemical kinetics have been simplified to the one-step reaction described by equation (1). A detailed consideration of the chemical kinetics for premixed combustion in porous media has been described by Hsu and Matthews [8] for a simple one-dimensional plug-flow situation. Their results suggest

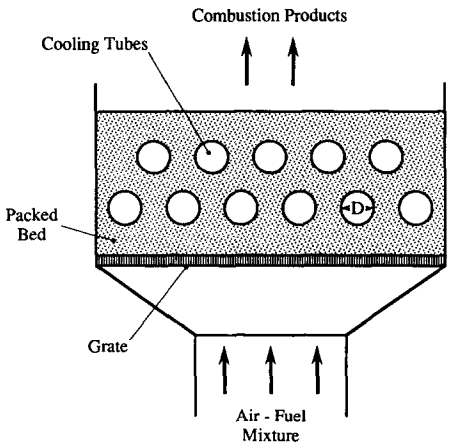

FIG. 1. Schematic diagram of the packed bed combustor–heater.

that the one-step kinetic model leads to an over prediction of the peak flame temperature.

The actual physical system is modelled as shown in Fig. 2. From symmetry considerations, calculations may be restricted to a single computational module that is representative of the entire domain. The location of the flame, indicated schematically on Fig. 2, is not assigned *a priori*, but is an outcome of the calculation. General features of the model include the calculation of radiation in the porous medium using a diffusion approximation (i.e. the thermal conductivity of the porous matrix is considered to be augmented by a radiative 'conductivity'). In addition, it is assumed that the gas and the solid matrix are in thermal equilibrium with each other, i.e. the temperature of the gas is equal to the temperature of the solid locally. Hence, an effective thermal conductivity is used to model the combined effects of gas and solid conductivity. Another distinguishing feature of the model is that gravitational (buoyancy) effects are fully

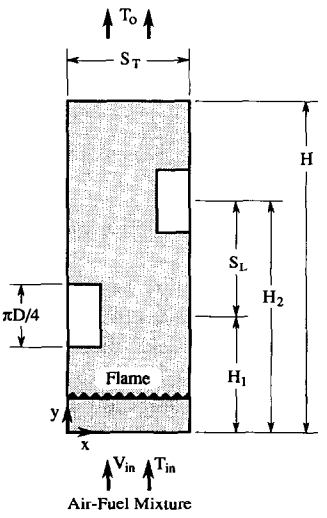

FIG. 2. Computational domain with the coordinate system.

taken into account and the commonly-used Boussinesq approximation is not invoked. The flow field is treated as being non-Darcian, with inertia and boundary effects modelled by the Forchheimer and Brinkman extensions to Darcy's equation [9]. The governing equations for two-dimensional steady state conditions can be written as:

Continuity

$$\frac{\partial}{\partial x}(\rho u)+\frac{\partial}{\partial y}(\rho v)=0 \tag{2}$$

x-momentum

$$\frac{\partial}{\partial x}(\rho uu)+\frac{\partial}{\partial y}(\rho vu)=-\frac{1}{\phi}\frac{\partial p}{\partial x}+\frac{\partial}{\partial x}\left(\mu\frac{\partial u}{\partial x}\right)+\frac{\partial}{\partial y}\left(\mu\frac{\partial u}{\partial y}\right)-\frac{\mu u}{K}-\rho f\frac{|\mathbf{v}|u\phi}{\sqrt{K}} \tag{3}$$

y-momentum

$$\frac{\partial}{\partial x}(\rho uv)+\frac{\partial}{\partial y}(\rho vv)=-\frac{1}{\phi}\frac{\partial p}{\partial y}+\frac{\partial}{\partial x}\left(\mu\frac{\partial v}{\partial x}\right)+\frac{\partial}{\partial y}\left(\mu\frac{\partial v}{\partial y}\right)-\frac{\mu v}{K}-\rho f\frac{|\mathbf{v}|v\phi}{\sqrt{K}}-\rho g \tag{4}$$

Energy

$$\frac{\partial}{\partial x}(\rho uh_f)+\frac{\partial}{\partial y}(\rho vh_f)=\frac{\partial}{\partial x}\left(\frac{k_{eff}}{c_{p_f}}\frac{\partial h_f}{\partial x}\right)+\frac{\partial}{\partial y}\left(\frac{k_{eff}}{c_{p_f}}\frac{\partial h_f}{\partial y}\right)+\Delta H_c S_{fu} \tag{5}$$

Mass fraction of fuel

$$\frac{\partial}{\partial x}(\rho um_f)+\frac{\partial}{\partial y}(\rho vm_f)=\frac{\partial}{\partial x}\left(\rho D_{AB}\frac{\partial m_f}{\partial x}\right)+\frac{\partial}{\partial y}\left(\rho D_{AB}\frac{\partial m_f}{\partial y}\right)-S_{fu} \tag{6}$$

where the rate of consumption of the fuel is given by a one-step Arrhenius rate equation [10, 11]

$$S_{fu}=A\rho^2 m_f m_{ox}\exp[-E/RT]. \tag{7}$$

The energy equation is expressed in terms of the fluid enthalpy, rather than the fluid temperature, to account for variations of the specific heat with temperature and species concentration. However, since the fluid temperature is needed for evaluation of the thermophysical properties, the enthalpy is related to the fluid temperature through a supplementary equation, as discussed in the following section. The large temperature variations in the computational domain result in large variations in density and viscosity. The advective terms on the left hand side of the two momentum equations are employed to account for

the flow acceleration caused by the density change. The Brinkman terms on the right hand side are similar in form to those employed for constant-viscosity situations. A justification for the chosen form of the momentum equations must await experimental confirmation.

Boundary conditions

The following boundary conditions are imposed on the solution:

$$\text{at } y = 0, \quad u = 0, \quad v = v_{in}, \quad h = h_{in}, \quad \text{and} \quad m_f = m_{f,in} \tag{8a}$$

$$\text{at } y = H, \quad \frac{\partial u}{\partial y} = \frac{\partial v}{\partial y} = \frac{\partial m_f}{\partial y} = 0 \tag{8b}$$

and

$$-k_{eff}\frac{\partial T}{\partial y} = (\varepsilon_{eff}\sigma T_f^4 - \alpha_{eff}\sigma T_{am}^4). \tag{8c}$$

Equation 8(c) expresses the fact that the surface of the packed bed radiates energy to the surrounding surfaces (that are at ambient temperature). The effective emissivity and absorptivity of the bed surface, ε_{eff} and α_{eff}, are assumed equal to simplify the solution. The effective emissivity is calculated from the known emissivity of the bed material and the known convoluted geometry of the free surface of the bed. At $x = 0$ and $x = W$, the symmetry conditions are imposed:

$$\frac{\partial v}{\partial x} = \frac{\partial h_f}{\partial x} = \frac{\partial m_f}{\partial x} = u = 0. \tag{8d}$$

At the surfaces of the tubes, the usual no-slip and impenetrability conditions are applied to the momentum equations, and the gradient of the mass fraction normal to the surface is set to zero. At the tube surface, the boundary condition for the energy equation involves a specification of the heat flux to the tube wall. The heat flux is computed from the expression

$$q = k_{eff}\frac{\partial T}{\partial n} = \frac{T - T_c}{R_t} \tag{8e}$$

where n is the outward normal to the tube surface, T_c is the temperature of the coolant within the tube, and R_t is the total thermal resistance between the bed and the coolant:

$$R_t = \frac{1}{h} + \frac{r_i \ln(r_o/r_i)}{k_{tube}} + R_{contact}. \tag{8f}$$

The numerical values of the quantities appearing in the foregoing equation are presented in Table 1.

Thermophysical properties

Since the temperature varies significantly through the packed bed (from about 300 K at the inlet to about 2000 K in the flame zone), it is necessary to consider variations of the thermophysical properties with temperature. The thermal conductivity and emissivity of alumina (Al_2O_3) are obtained from polynomial curve fits to published data [12, 13]. For simplicity, the thermal conductivity and viscosity of the gas are approximated by the values for nitrogen, and curve fits of the form of Sutherland's correlation are used [14].

Table 1. Operating conditions

Quantity	Value
Activation energy (J kmol^{-1})	1.4×10^8
Bed height, H (mm)	120.65
Bed width, S_T (mm)	12.7
Contact resistance between porous matrix and cooling tube walls (m^2 K W^{-1})	0.003
Cooling water temperature (K)	291
Excess air	10%
Firing rate (kW)	45
Heat transfer coefficient inside the cooling tubes (W m^{-2} K^{-1})	2725
Height of first tube row, H_1 (mm)	57.15
Height of second tube row, H_2 (mm)	95.25
Inlet gas temperature (K)	301
Particle diameter (mm)	6.0
Porosity	0.43
Tube diameter (mm)	12.7

The effective thermal conductivity of the porous medium is calculated under the assumptions that the medium is a continuum and the temperature of the gas and the solid matrix are equal locally. The following expression is employed [15]:

$$k_{eff} = k_{con} + k_{dis} + k_{rad} \tag{9}$$

where the effective thermal conductivity is the sum of the conductivities due to conduction, dispersion and radiation and can be expressed, respectively, as

$$k_{con} = \frac{2k_f}{1 - (k_f/k_s)}\left[\frac{\ln(k_s/k_f)}{1 - (k_f/k_s)} - 1\right] \tag{10}$$

$$k_{dis} = 0.0895 Pr\left(\frac{\rho V d_p}{\mu}\right)k_f \tag{11}$$

and

$$k_{rad} = 0.707 k_f (k_s/k_f)^{1.11}\left[\frac{4\sigma T^3}{2\left(\frac{1}{\varepsilon_s} - 1\right) + \frac{1}{F_{12}}}\frac{d_p}{k_s}\right]^{0.96} \tag{12}$$

where F_{12} is the radiation view factor between two contacting spheres.

It is appropriate to note that the assumption of thermal equilibrium between the gas and solid phases is questionable if the particle diameter is large. This issue will be considered in detail in a subsequent paper. The validity of the continuum approximation employed in this model is also questionable if the particle diameter is large. However, the alternative to the continuum model is to attempt to resolve the flow field within the porous structure—a prohibitively cumbersome undertaking. To model the thermal con-

Table 2. Correlating equations for enthalpy and specific heat; $Z = [(T-1400)/200]$, $\psi = a+bz+cz^2+dz^3+ez^4+fz^5$

ψ	a	b	c	d	e	f
$c_{p,a}$	1206.034318	22.779916	−3.455606	0.426062	0.042889	−0.011736
$c_{p,g}$	1401.65961	36.60067	−4.4302	0.316066	0.046715	−0.0099
h_a	1.234164	0.243788	0.003322	−0.000059	0.000041	0.00006
h_g	1.399955	0.28089	0.004526	0.000402	0.000224	0.000023

Units: c_p [J kg^{-1} K^{-1}], h [MJ kg^{-1}].

tact resistance and porosity variations at the grate, the effective thermal conductivity given by equation (9) is reduced by a factor of 0.3 in this region. The reduction factor was established by matching the prediction to the measured data at one operating condition.

Following Rhine and Tucker [16], the enthalpy of air (h_a) and of the products of stoichiometric combustion of methane (h_g) can be correlated as functions of temperature. The polynomial curve fits presented by them are given in Table 2. As suggested by them, the enthalpy of the gaseous mixture of combustion products and air is related to the temperature through the following formula:

$$h_f = [(R_s\rho_a^\circ+\rho_g^\circ)h_g + (R_x-R_s)\rho_a^\circ h_a]/(\rho_a^\circ R_x+\rho_g^\circ). \quad (13)$$

Because equation (13) is nonlinear, the Newton–Raphson method is used to solve for the temperature field from the known enthalpy field. Table 2 also contains polynomial curve fits for specific heats of air and the products of combustion. These formulas are used to calculate the specific heat of the gaseous mixture for use in equation (5).

Method of solution

The model equations, together with appropriate boundary conditions, are solved using a control volume finite difference approach [17]. To maintain simplicity in the finite-difference solution scheme to be adopted, the circular tubes are replaced by square ducts of equivalent perimeter. The iterative procedure for treatment of the coupled momentum and continuity equations, embodied in the SIMPLER algorithm [17], is used in the solution of the model equations. The solution procedure begins with a guess for the flame location. It is assumed that the entire heat release due to combustion occurs uniformly in the control volumes corresponding to the specified flame location. The mass, momentum, energy and species conservation equations are solved based on the guessed heat release distribution. After a few iterations, the computed species distribution is used to re-specify the heat release distribution, which is then held fixed for the next few iterations. This procedure is repeated every four iterations, except at the beginning, when ten iterations are carried out before updating the flame location. Fewer than 200 iterations are required to obtain full convergence for most cases. Fine meshes are used and each control volume is kept smaller than 0.4 mm in the x-direction and 0.8 mm in the y-direction. The number of nodes adopted depends on the geometry and the maximum temperature in the porous medium. Computational grids ranging from 35×151 to 55×251 nodes are used in x- and y-directions, respectively, to establish that the solutions are grid-independent. The iterations are terminated when the global energy and fuel balances are satisfied within the round-off error of the computer.

The heat absorbed by the cooling tube is calculated as

$$q_{tub} = \int_0^S \left(\frac{T(x,y)-T_w}{R_t}\right) dS \quad (14)$$

where S is the surface area of the tube, and R_t is the total thermal resistance between the tube and the coolant, defined by equation (8f). The baseline operating conditions for the present studies are summarized in Table 1. The parametric calculations to be presented involve variations of individual parameters from the baseline conditions.

Dimensionless parameters

If the thermophysical properties appearing in the governing equations (2)–(6) are assumed to be constants, the equations can be nondimensionalized with tube diameter, inlet velocity and enthalpy of combustion as scales for length, velocity and enthalpy, respectively. The reduction of the equations to dimensionless form is, of course, of limited utility, in view of the large property variations involved. However, at least a partial grasp on the large number of variables governing the problem can be obtained through the process. The non-dimensional governing equations can be written as:

$$\frac{\partial}{\partial\xi}(UU)+\frac{\partial}{\partial\eta}(VU) = -\frac{1}{\phi}\frac{\partial P}{\partial\xi} + \frac{1}{Re}\left(\frac{\partial^2U}{\partial\xi^2}+\frac{\partial^2U}{\partial\eta^2}\right)-\frac{U}{Re\,Da}-\frac{f\phi|\mathbf{V}|U}{\sqrt{Da}} \quad (15)$$

$$\frac{\partial}{\partial\xi}(UV)+\frac{\partial}{\partial\eta}(VV) = -\frac{1}{\phi}\frac{\partial P}{\partial\eta} + \frac{1}{Re}\left(\frac{\partial^2V}{\partial\xi^2}+\frac{\partial^2V}{\partial\eta^2}\right)-\frac{V}{Re\,Da}-f\phi\frac{|\mathbf{V}|V}{\sqrt{Da}}-\frac{1}{Fr^2} \quad (16)$$

$$\frac{\partial}{\partial\xi}(UH_f)+\frac{\partial}{\partial\eta}(VH_f)=\frac{1}{Pe}\left(\frac{\partial^2 H_f}{\partial\xi^2}+\frac{\partial^2 H_f}{\partial\eta^2}\right)+S^*_{fu} \tag{17}$$

$$\frac{\partial}{\partial\xi}(Um_f)+\frac{\partial}{\partial\eta}(Vm_f)=\frac{1}{Sc\,Re}\left(\frac{\partial^2 m_f}{\partial\xi^2}+\frac{\partial^2 m_f}{\partial\eta^2}\right)-S^*_{fu}. \tag{18}$$

In addition to the parameters ϕ, Re, Da, Fr, Pe, Sc, and S^*_{fu}, there are geometrical ratios, such as H/D, S_L/D, S_T/D and tube shape (circular, elliptical, etc.). The composition of the reactant stream at the inlet is described by the excess air (ψ).

An important variable, that is embedded in several of the foregoing dimensionless groups, is the particle diameter. The particle diameter plays a major role in heat transfer between the bed and the cooling tube and pressure drop across the bed. Therefore, the geometrical ratio d_p/D should be viewed as a primary dimensionless parameter. For the continuum model to be valid, it is necessary that $d_p/D < 1$.

The formidable number of dimensionless parameters precludes an exhaustive investigation of the effect of each variable. The present work is, therefore, limited to an examination of the effects of some of the more important parameters on the performance of the combustor–heater system.

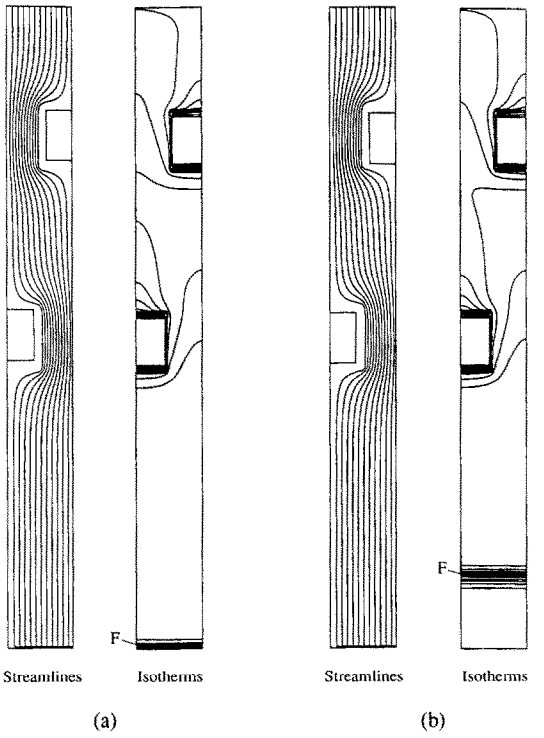

FIG. 3. Streamlines and isotherms (a) excess air of 10%, (b) excess air of 50%; F represents location of maximum heat release by combustion.

RESULTS AND DISCUSSION

The purpose of the numerical simulations is to predict the thermal efficiency, flame location, temperature distribution and pressure drop in the combustor–heater. The effects of the excess air, firing rate, particle diameter, tube spacing, activation energy and the effective thermal conductivity are addressed in this work. Other parameters, such as the shape of the tubes, possible alternative tube arrangements, and the type of porous material are not considered. The results are presented for a packed bed of spherical alumina (Al_2O_3) particles in which two staggered tube rows are embedded. The thermal efficiency of the combustor–heater is defined as the ratio of heat absorbed by the grate and the tubes to the heat released by combustion. The following subsections discuss the effects of the aforementioned parameters on the thermal efficiency, pressure drop, maximum temperature, and outlet temperature of the gas. Whenever possible, the predictions are compared with available experimental data.

Effect of excess air

A pictorial impression of the flow field and temperature distribution in the combustor–heater is provided by the steamlines and isotherm contour plots shown in Figs. 3(a) and (b) for excess air of 10 and 50%, respectively. In contrast to the flow pattern that would be expected if the particles were not present, the streamlines reveal that there is no recirculating flow in the wakes of the tubes. The closely-packed isotherms near the grate indicate the flame zone. The temperature is rather uniform in the region downstream of the flame zone, indicating that the region between the flame and the first tube row is thermally passive. Comparison of Figs. 3(a) and (b) shows that the flame stabilizes farther from the grate as the excess air is increased.

For a fixed fuel flow rate, Fig. 4 presents the variations of the maximum temperature in the bed as well

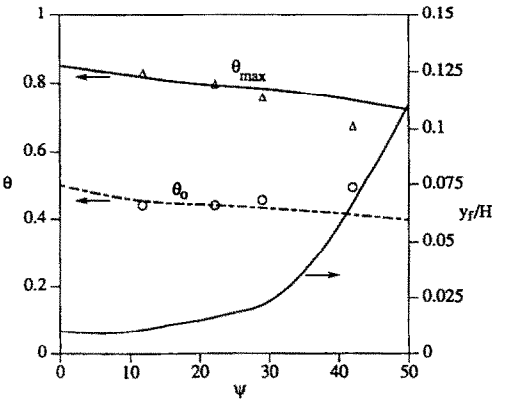

FIG. 4. Effect of excess air on the flame temperature, outlet temperature and flame location.

as the outlet temperature of the gas with variations in the excess air. As might be expected, both temperatures diminish as the excess air is increased. The figure also depicts the variation of the flame location (as defined by the peak of heat release by the combustion) with excess air. Consistent with the trend suggested by Fig. 3, the flame location is found to be strongly influenced by the excess air. Increases in excess air cause the flame zone to move downstream. The effect of excess air on the performance of the combustor–heater has been studied experimentally by Xiong and Viskanta [18], and their data is included in the figure for comparison with the predictions of the model. The measured values of the maximum and outlet temperatures are found to be in good agreement with the predictions except at the highest experimental excess air ratio, 42%. For this condition, the predicted peak flame temperature is too high, while the outlet temperature is too low. Insight on the reason for the discrepancy will be obtained by an examination of the next figure.

Figure 5 presents ratios of the heat absorbed by the grate, the first row of tubes, the second row of tubes and the total energy absorbed to the total heat released by combustion. The ratios are expressed as percentages and plotted along with experimental data against the percentage of excess air in the reactant mixture. The predicted results are comparable with experimental data within acceptable deviations ($\pm 15\%$) for the three lower values of excess air, while the data for an excess air of 42% deviate significantly from the predicted results. Temperature measurements by Xiong and Viskanta suggested that for excess air of 42% the flame stabilizes between the first and second row of tubes, whereas the prediction shows that the flame stabilizes between the grate and first row of tubes, although far away from the grate. Since the predicted flame location is upstream of the first row of tubes, it is understandable that the predicted total heat transfer rate exceeds the experimentally measured rate. Consequently, the predicted outlet temperature is lower than the experimental value. It is also understandable that the peak temperature associated with a flame stabilized in the thermally passive zone between the grate and the first tube row would be higher than that of a flame stabilized between the two tube rows. To ascertain whether the predicted flame location was dependent on the initially guessed location and whether it was possible to predict a stable flame in the space between the tube rows, a trial was conducted in which the flame was initially specified to lie between the tube rows. The flame was extinguished after a few iterations.

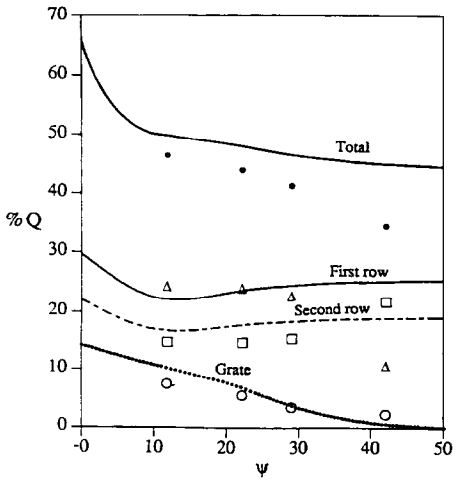

FIG. 5. Effect of excess air on the heat transfer rates.

For comparison, a simulation was performed for a duct with staggered tube rows, for the same geometry as shown in Fig. 2, but without a porous matrix in the duct. The predicted thermal efficiency was only 15.3% compared with 50.1% for a system with tubes embedded in the porous matrix. The porous medium enhances the thermal efficiency of the system because it greatly increases heat transfer both through direct thermal conduction and radiation. The reader is cautioned that the foregoing comparison may be skewed in favor of the porous matrix system, because the flow in the empty duct was assumed to be laminar. Nevertheless, it is reasonable to expect sizable heat transfer enhancement with the porous medium.

Effect of firing rate

The effect of the firing rate on the thermal efficiency of the combustor–heater has been investigated experimentally by Xiong and Viskanta [18]. The predicted thermal efficiency and average heat flux are compared with experimental data in Fig. 6. The average heat flux is calculated as the total thermal energy extracted divided by the total area of heat transfer surface of the tubes and grate. While the predicted trends are consistent with the experimental data, and the deviation between the data and predictions is about 15% which is within acceptable engineering accuracy, the numerical predictions overestimate the thermal efficiency and the average heat flux. One of the reasons may be due to heat losses from the test apparatus, which increase as the firing rate increases due to increased heat transfer to the ambient. Also, incorrect

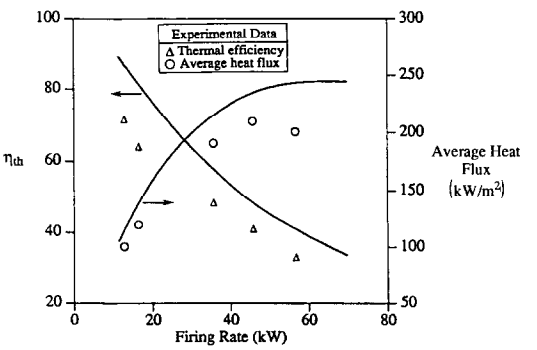

FIG. 6. Effect of firing rate on the overall heat transfer and thermal efficiency.

modelling of the contact resistance between the heat transfer surfaces and the particles may contribute to this dependency. Finally, the porosity variation near the tube wall is another complicating factor that has not been taken into account in the model.

Effect of particle diameter

Inspection of equations (3) and (4) shows that the Darcy and Forchheimer source terms are affected by the permeability, which is dependent on the particle diameter. In the absence of a velocity gradient, the permeability only affects the pressure drop; however, in the present system, the permeability also affects the velocity distribution, and hence, the temperature field. In addition, as suggested by equations (11) and (12), both the dispersive and the radiative contributions to the effective conductivity increase as the particle diameter increases. Since the effect of the particle diameter on the pressure, velocity and temperature fields is significant, an exploration of the effect of varying the particle size is important.

Figure 7 shows the effect of the particle diameter on the thermal efficiency and pressure drop. Increasing the particle diameter increases the thermal efficiency and decreases the pressure drop significantly. The thermal efficiency increases from 33.5 to 50.1% as the particle diameter increases from 1 to 6 mm for a 12.7 mm diameter tube. The pressure drop approaches the value that would be predicted for a packed bed without the tubes, as d_p/D approaches unity.

Increasing the ratio d_p/D has a favorable effect on the temperature field (Fig. 8). The maximum and outlet temperatures drop as the particle diameter is increased. Since the formation of NO_x decreases as the temperature decreases, a large particle diameter is desirable. The flame location is not affected by the particle diameter for $d_p/D > 0.2$, but an effect is observed for smaller particle diameters.

Figure 9 shows that the fraction of energy transferred to the grate increases as the particle diameter increases, due to the increased energy transport by radiation and dispersion. For $d_p/D > 0.2$, the fraction

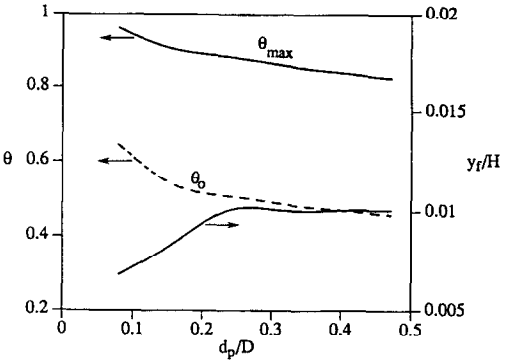

FIG. 8. Effect of particle diameter on the flame temperature, outlet temperature and flame location.

of energy absorbed by the first and the second rows of cooling tubes is not affected significantly. This can be explained by inspection of the variation of the temperature field in the packed bed. Increasing the particle diameter from 2 to 6 mm increases the effective thermal conductivity by a factor greater than two. Correspondingly, the heat absorbed by the grate increases and the flame temperature decreases (by about 150 K). The larger effective thermal conductivity associated with the larger particle is offset by the decrease in the temperature, and, hence, the heat absorbed by the tube rows is not affected significantly by the increase in the particle diameter. An additional factor resulting in the insensitivity of tube heat transfer is the controlling effect of contact resistance between the particles and tubes.

Effect of tube spacing

To study the effect of the vertical spacing between tube rows, the location of the first row of tubes is held fixed while the location of the second tube row is changed vertically. To study the effect of the horizontal spacing, the transverse pitch of both tube rows is adjusted. The effect of horizontal spacing on the thermal efficiency and pressure drop are shown in Fig.

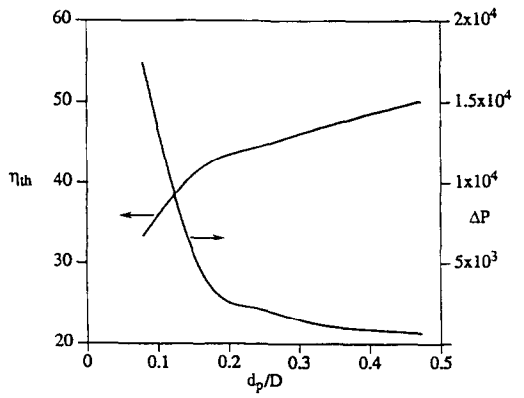

FIG. 7. Effect of particle diameter on the thermal efficiency and pressure drop.

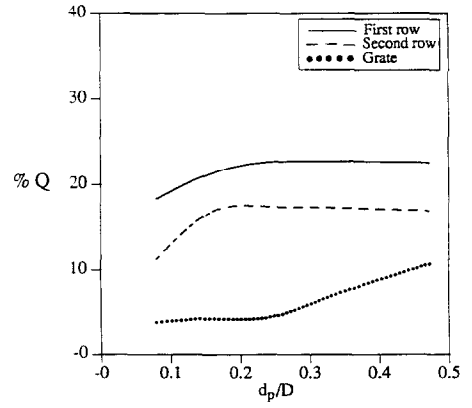

FIG. 9. Effect of particle diameter on the fraction of heat absorbed by grate and tube rows.

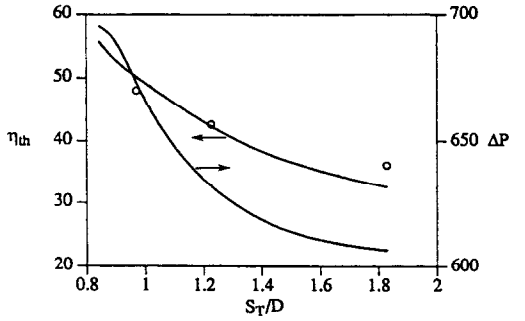

FIG. 10. Effect of horizontal spacing between rows on the thermal efficiency and pressure drop.

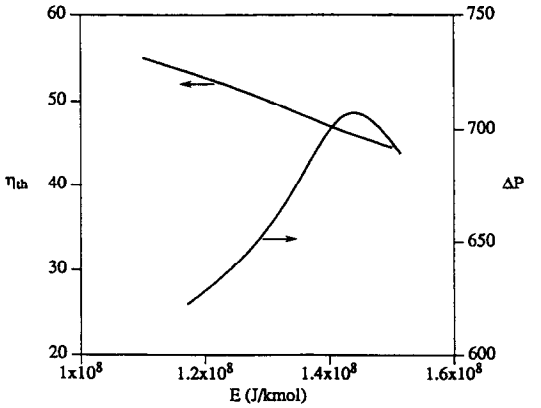

FIG. 12. Effect of activation energy on the thermal efficiency and pressure drop.

10 for a fixed firing rate. Since bringing the tubes closer together increases the local velocities, both the rate of heat transfer to the tubes and the pressure drop increase. The predicted thermal efficiencies are in good agreement with the measured values presented by Xiong and Viskanta. As shown in Fig. 11, the horizontal spacing does not have a significant effect on the flame zone temperature, but increasing the horizontal spacing increases the amount of gas that bypasses the coolant tubes and increases the outlet temperature. Therefore, increasing the horizontal spacing may increase the NO_x formation. The flame location is changed very little as S_T/D changes at relatively low excess air operation.

The vertical spacing between tube rows has little influence on the temperature, heat transfer rates, and pressure drop.

Effect of activation energy

The activation energy of the fuel is usually determined experimentally, and the results may suffer from uncertainty. The composition of natural gas depends on the site and source. Therefore, the activation energy of natural gas is not the same as for pure methane and may change with natural gas from location to location. The purpose of this subsection is to study the sensitivity of the model as the activation energy is changed by $\pm 20\%$ from the value 1.5×10^8 J kmol^{-1} reported for pure methane [11].

As revealed by Figs. 12 and 13, the thermal efficiency, temperature field and flame location are significantly affected as the activation energy is changed from 1.0×10^8 to 1.6×10^8 J kmol^{-1}. The flame moves away from the grate as the activation energy increases, and the overall thermal efficiency decreases. It is found that at an activation energy of 1.6×10^8 J kmol^{-1} the rate of heat transfer to the grate decreases to near zero. The maximum temperature and the outlet temperature increase as the activation energy increases (Fig. 13). The pressure drop increases with the activation energy up to $E = 1.5 \times 10^8$ J mol^{-1} and slightly decreases thereafter. The temperature of the gas mixture ahead of the flame is almost equal to the inlet temperature, and the velocity is also equal to the inlet velocity. The pressure drop in this region is small compared with that in the high temperature region. The temperature in the flame and post flame zone may be of the order of 2000 K, and the gas expands significantly. This increases the velocity by a factor of ten and causes an increase in the pressure

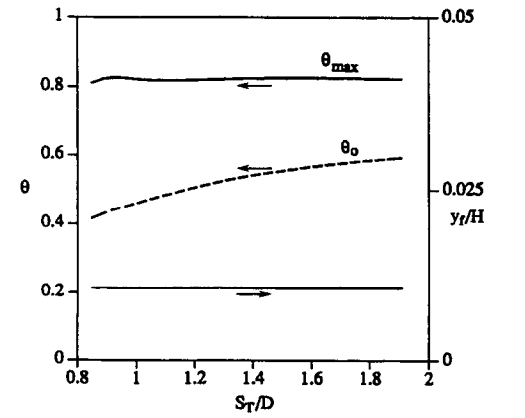

FIG. 11. Effect of horizontal spacing between tube rows on the flame temperature, outlet temperature and flame location.

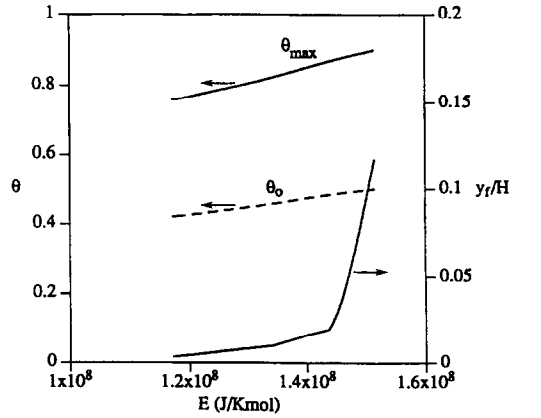

FIG. 13. Effect of activation energy on the flame temperature, outlet temperature and flame location.

drop. This may explain why the pressure drop decreases slightly as the flame moves to $y_f/H > 0.1$, since the region ahead of the flame does not suffer from a significant pressure drop.

Effect of the effective thermal conductivity

As discussed earlier, the predictions overestimate the rate of heat transfer (see Figs. 5 and 6). The overestimate may possibly result from an inaccurate modelling of the effective thermal conductivity. The available literature on the effective thermal conductivity reveals there are large differences among the different thermal conductivity models. To determine how the uncertainty in the modeling of the thermal conductivity affects the prediction of the performance, the effective thermal conductivity used in the model (equation (5)) is decreased and increased by 50%. The results show that an increase in the thermal conductivity by 50% increases thermal efficiency from 50.1 to 55.4%, and decreasing the thermal conductivity decreases the thermal efficiency from 50.1 to 40.8%. In addition, the thermal conductivity is found to have an effect on the flame thickness. An increase in the thermal conductivity spreads the flame, i.e. increases the width of the combustion zone.

CONCLUSIONS AND RECOMMENDATIONS

A mathematical model has been developed, and numerically obtained results compared with available experimental data for a porous matrix combustor–heater. Thermal efficiency, temperature distribution, flame location and pressure drop have been predicted for a range of design and operating parameters and system configurations. Numerical results compare reasonably well with the available experimental data and are within acceptable engineering accuracy ($\pm 15\%$). The following conclusions can be drawn from the predicted results.

- Increasing the excess air ratio decreases the thermal efficiency and decreases the temperature of the exhaust gas. The flame location is a strong function of the excess air. An increase in the excess air stabilizes the flame far from the grate.
- The particle diameter of the bed material has a significant effect on the thermal performance of the combustor–heater. Increasing the particle diameter, within the range studied, increases the thermal efficiency and decreases the pressure drop. In addition, increasing the particle diameter reduces the maximum temperature, thereby potentially decreasing the formation of NO_x.
- Horizontal spacing of the staggered tubes significantly affects the thermal efficiency of the heater. Decreasing the horizontal spacing increases the thermal efficiency and reduces the maximum temperature. The vertical spacing, however, is not a significant design parameter influencing performance of the combustor heater.
- Changing the activation energy within the uncertainty range affects the performance of the combustor significantly, because the flame location is a strong function of the activation energy.
- In order to obtain more accurate predictions it is necessary to model the effective thermal conductivity and contact resistance between the embedded tubes and the porous bed in addition to the porosity variation near the walls.

Acknowledgements—The work was supported jointly by the Gas Research Institute, under contract No. 5090-260-1927, and Institute of Gas Technology's sustaining membership program. The authors would like to acknowledge numerous discussions with Mr M. J. Khinkis and Dr T. Y. Xiong of IGT concerning modelling of the porous-matrix combustor heater and would like to thank Dr F. Fish of the Gas Research Institute for his interest and support.

REFERENCES

1. R. Echigo, Radiation enhanced/controlled phenomena of heat and mass transfer in porous media, *Proceedings of the Third ASME/JSME Joint Thermal Engineering Conference* (Edited by J. R. Lloyd and Y. Kurosaki), Vol. 6, pp. 361–366. ASME, New York (1991).
2. Y. Yoshizawa, K. Sasaki and R. Echigo, Analytical study of the structure of radiation controlled flame, *Int. J. Heat Mass Transfer* **31**, 311–319 (1988).
3. R. Viskanta, Enhancement of heat transfer in industrial combustion systems: problems and future challenges, *Proceedings of the Third ASME/JSME Joint Thermal Engineering Conference* (Edited by J. R. Lloyd and Y. Kurosaki), Vol. 5, pp. 161–173. ASME, New York (1991).
4. M. J. Khinkis, W. Kunc and T. Y. Xiong, Advanced gas-fired ultra-low emissions surface combustor heater, Paper presented at the American Flame Research Committee (AFRC), 1989 International Symposium on Combustion in Industrial Furnaces and Boilers, Short Hills, NJ (1989).
5. C. Chaffin, M. Koeing, M. Koeroghlian, R. D. Matthew, M. J. Hall, S. P. Nichols and I.-G. Lim, Experimental investigation of premixed combustion within highly porous media, *Proceedings of the Third ASME/JSME Joint Thermal Engineering Conference* (Edited by J. R. Lloyd and Y. Kurosaki), Vol. 4, pp. 219–224. ASME, New York (1991).
6. Y.-K. Chen, R. D. Matthews and J. R. Howell, The effect of radiation on the structure of premixed flame within a highly porous media, ASME-HTD Vol. 81, pp. 35–44. ASME, New York (1987).
7. A. A. Mohamad and R. Viskanta, Combined convection radiation heat transfer in a surface combustor-process heater. In *Simulation of Thermal Energy Systems* (Edited by R. F. Boehm and Y. M. El-Sayed), HTD Vol. 124, pp. 1–8. ASME, New York (1989).
8. P.-F. Hsu and R. D. Matthews, The necessity of using detailed kinetics in models for premixed combustion within porous media, *Combust. Flame* **93**, 457–466 (1993).
9. M. Kaviany, *Principles of Heat Transfer in Porous Media*. Springer, New York (1991).
10. K. K. Kuo, *Principles of Combustion*. Wiley, New York (1986).
11. A. M. Kanury, *Introduction to Combustion Phenomena: for Fire, Incineration, Pollution, and Energy Applications*. Gordon and Breach, London (1985).
12. Y. S. Touloukian, R. W. Powell, C. Y. Ho and P. G. Klemens, *Thermal Conductivity, Nonmetallic Solids*, Vol. 2, p. 119. IFI/Plenum, New York (1970).

13. Y. S. Touloukian and D. P. DeWitt, *Thermal Radiation Properties, Nonmetallic Solids*, p. 142. IFI/Plenum, New York (1972).
14. R. W. Fox and A. T. McDonald, *Introduction to Fluid Mechanics* (3rd Edn). Wiley, New York (1985).
15. N. Wakao and S. Kaguei, *Heat and Mass Transfer in Packed Beds*. Gordon and Breach, London (1982).
16. J. M. Rhine and R. J. Tucker, *Modeling of Gas-Fired Furnaces and Boilers*. McGraw-Hill, London (1991).
17. S. V. Patankar, *Numerical Heat Transfer and Fluid Flow*. Hemisphere, New York (1980).
18. T.-Y. Xiong and R. Viskanta, A basic study of porous-matrix combustor-heater. In *Fossil Fuels Combustion*—1992 (Edited by R. Ruiz), PD.-Vol. 39, pp. 31–39. ASME, New York (1992).